

Qimax: Efficient quantum simulation via GPU-accelerated extended stabilizer formalism

Vu Tuan Hai^{1,2*}, Bui Cao Doanh³, Le Vu Trung Duong³,
Pham Hoai Luan³, Yasuhiko Nakashima³

^{1*}University of Information Technology, Ho Chi Minh city, 700000, Vietnam.

^{2*}Vietnam National University, Ho Chi Minh city, 700000, Vietnam.

^{3*}Nara Institute of Science and Technology, 8916-5 Takayama-cho, Ikoma, 630-0192, Nara, Japan.

*Corresponding author(s). E-mail(s): haivt@uit.edu.vn;

Abstract

Simulating Clifford and near-Clifford circuits using the extended stabilizer formalism has become increasingly popular, particularly in quantum error correction. Compared to the state-vector approach, the extended stabilizer formalism can solve the same problems with fewer computational resources, as it operates on stabilizers rather than full state vectors. Most existing studies on near-Clifford circuits focus on balancing the trade-off between the number of ancilla qubits and simulation accuracy, often overlooking performance considerations. Furthermore, in the presence of high-rank stabilizers, performance is limited by the sequential property of the stabilizer formalism. In this work, we introduce a parallelized version of the extended stabilizer formalism, enabling efficient execution on multi-core devices such as GPU. Experimental results demonstrate that, in certain scenarios, our Python-based implementation outperforms state-of-the-art simulators such as Qiskit and PennyLane.

Keywords: quantum simulation, stabilizer, CUDA, Cupy

1 Introduction

Simulating a quantum system classically demands significant resources, scaling exponentially with the number of particles, posing a challenging computational problem. For instance, Google’s quantum computer, Sycamore, demonstrated quantum supremacy by producing results in days that would take classical computers thousands of years to simulate [1]. Various simulation methods have been proposed, including state-vector [2], tensor-network [3], decision diagram [4], and stabilizer formalism [5]. Each method offers different levels of fidelity and resource requirements depending on the quantum circuit’s size and type.

Quantum simulator development aims to address domain-specific and general-purpose applications, ultimately targeting the boundary of quantum advantage, where classical computers cannot simulate quantum systems within a acceptable execution time. Simulator scalability is assessed by the number of qubits (n , or #Qubits) and gates (m , or #Gates). In the state-vector approach, the quantum state $|\psi(\boldsymbol{\theta})\rangle$ is represented as a 2^n -dimensional complex tensor, leading to an exponential increase in execution time and memory requirements with #Qubits, while #Gates affects execution time linearly. This exponential scaling is inherent to quantum systems in the state-vector approach. Recent stabilizer formalism research focuses on reducing gate application times for Clifford circuits.

Stabilizer formalism based on Heisenberg’s picture provides a compact representation for quantum systems and gate applications where the quantum system can be described as stabilizers. Quantum gates act on the stabilizers by mapping between n -qubit Pauli string \mathcal{P}_n rather than matrix-vector multiplication. Existing stabilizer formalism packages have been developed, although they can run a hundred-qubit Clifford circuit with a million gates, the stabilizer formalism limits the application of the quantum simulator, especially for algorithms that require non-Clifford gates. On the other hand, using non-Clifford gates in (extended) stabilizer formalism may lead to a fast increase in complexity. For instant, [6] shows the exponential rise of stabilizer rank in cases of QNN, which require non-Clifford gates. Other studies address this by employing approximation methods, balancing complexity and accuracy [7].

There are two use cases of stabilizer formalism: (1) large-qubit Clifford circuits, and (2) low-rank Clifford and non-Clifford. Because Stim [8] effectively handles the first, our research focuses on the second. Clifford circuits are only used for quantum error correction and benchmarking the performance of quantum hardware. Near-Clifford circuits have wider applications. Table 1 summarizes recent stabilizer and extended stabilizer formalism packages, revealing that all prior extended stabilizer packages rely on sequential algorithms, limiting their performance on GPUs. Our proposed package, Qimax, addresses this limitation by offering three modes: v1 (standard extended stabilizer formalism, CPU-based), v2 (parallel stabilizer formalism, GPU-based, using one-hot vector Pauli encoding), and v3 (parallel stabilizer formalism, GPU-based, using tensor index encoding).

Package	Interface	Backend	Property	Gate set	Dependence	Release year
stim [8]	Python	C++	Sequential	Clifford		2021
PyClifford	Python	Python	Sequential	Clifford	Qiskit [2], Pyscf	2022
QuiZX [9]	Python	Rust	Sequential	Clifford + non Clifford	ZX Calculus [10]	2022
WMC [6]	Python	Python	Sequential	Clifford + non Clifford	GPMC solver, d4max solver	2024
QuaSARQ [11]	C++	C++ (CUDA)	Parallel	Clifford		2025
Qimax	Python	Python	Sequential or Parallel	Clifford + non Clifford	CuPy [12]	2025

Table 1 Survey existing quantum simulator package based on stabilizer formalism

2 Background

2.1 Extended stabilizer formalism

An n -qubit quantum state $|\psi\rangle$ is defined as a stabilizer state by an operator U if and only if it is a +1 eigenvector of U , meaning $U|\psi\rangle = |\psi\rangle$. The stabilizer states form a strict subset of all quantum states that can be uniquely described by the stabilizer group $\{\mathcal{P}_n\}$. The elements of the stabilizer group are called stabilizers. Any stabilizer group can be specified by a set of generators $G_{|\psi\rangle} \equiv G = \{\mathbb{P}_n\}$ so that every element in the stabilizer group can be obtained through matrix multiplication between any pair $\{\mathbb{P}_{n,i}, \mathbb{P}_{n,j}\}$. The number of generators (order) of G is always n . These generators evolve under the application of m quantum gates, as shown in Equation (1):

$$G^{(0)} = \left\langle \begin{array}{c} \mathbb{P}_{n,0}^{(0)} \\ \vdots \\ \mathbb{P}_{n,n-1}^{(0)} \end{array} \right\rangle \xrightarrow{g^m} G^{(m)} = \left\langle \begin{array}{c} \mathbb{P}_{n,0}^{(m)} \\ \vdots \\ \mathbb{P}_{n,n-1}^{(m)} \end{array} \right\rangle, \quad (1)$$

where $\mathbb{P}_{n,j}^{(0)} \equiv \mathbb{Z}_{n,j} = I^{\otimes j} \otimes Z \otimes I^{\otimes(n-j-1)}$ and $G^{(0)}$ is the set of generator for initial state $|0\rangle^{\otimes n}$. Gate $g^{(t)}$ update $\mathbb{P}_{n,j}^{(t)}$ to $\mathbb{P}_{n,j}^{(t+1)}$ following by Table. B1, see Example. 1.

To achieve universal quantum computation, non-Clifford gates, such as rotation gates, must be included. These gates transform stabilizer states into non-stabilizer states. A generator may transform from a single Pauli string into a linear combination of Pauli strings:

$$\mathbb{P}_n = \sum_j \lambda_j P_{n,j} \quad (2)$$

with $\lambda P_n = \lambda p_0 \otimes \dots \otimes p_{n-1}$, $\equiv \lambda p_0 \dots p_{n-1}$ where $\lambda \in \mathbb{R}$ is the weight and P_n is the n -qubit Pauli string which is composed from n Pauli matrices $p_j \in \{I, X, Y, Z\}$.

Example 1 Consider a 3-qubit circuit $CX_{0,1}R_z(\pi/3)_0SX_0|000\rangle$. The evolution of the stabilizer generators G is tracked gate by gate, as specified in Table B1. For instance, the Pauli string $-Y$ is converted to $(\frac{1}{2}X - \frac{\sqrt{3}}{2}Y)$:

$$\left\langle \begin{array}{c} Z_{3,0} \\ Z_{3,1} \\ Z_{3,2} \end{array} \right\rangle \xrightarrow{SX_0} \left\langle \begin{array}{c} -YII \\ IZI \\ IIZ \end{array} \right\rangle \xrightarrow{R_z(\frac{\pi}{3})_0} \left\langle \begin{array}{c} \frac{1}{2}XII - \frac{\sqrt{3}}{2}YII \\ IZI \\ IIZ \end{array} \right\rangle \xrightarrow{CX_{0,1}} \left\langle \begin{array}{c} \frac{1}{2}XXI - \frac{\sqrt{3}}{2}YXI \\ ZZI \\ IIZ \end{array} \right\rangle \quad (3)$$

We can relate $G^{(m)}$ directly to the target density operator either as a product of stabilizers or as a sum of Pauli operators, as shown in (4), respectively:

$$\rho^{(m)} \equiv |\psi^{(m)}\rangle\langle\psi^{(m)}| = \frac{1}{2^n} \prod_{j=1}^n (I^{\otimes n} + \mathbb{P}_{n,j}^{(m)}) = \frac{1}{2^n} \sum_{\mathcal{P}_n \in \mathcal{P}|\psi} \lambda_{\mathcal{P}_n} \mathcal{P}_n. \quad (4)$$

In the other cases, we can simply track G to get measurement value as $p_{j,k} = \text{tr}([\frac{1}{2}(I^{\otimes n} + Z_k)]|\psi\rangle\langle\psi|)$, see Appendix. C for detail.

2.2 Gate set

The current generation of quantum computers such as IBM Quantum Heron, IBM quantum Eagle, Rigetti Anka-3 use a native gate set that include $\{I, X, SX, R_z(\theta)/R_x(\theta), CZ/ISWAP\}$. These is only one non-Clifford gate which can build any other gate using the circuit transpiler. Qimax is not only these basic gates, but also supports other gates with simple modifications in `create_LUT()` function. The Qimax's gate set used in this paper including $\{H, S, CX, R_x(\theta), R_y(\theta), R_z(\theta)\}$. The 3- and 4-qubit gates will be considered in the future version.

If a Clifford gate g is applied to the stabilizer state, then $UP_nU^\dagger g|\psi\rangle = g|\psi\rangle$. To be specific, a Clifford gate act on j^{th} qubit (denoted as g_j) in the stabilizer $\mathcal{P}_n = \lambda p_0 \otimes \dots \otimes p_{n-1}$, it return $g_j \mathcal{P}_n g_j^\dagger = \sum \lambda p_0 \otimes \dots \otimes g_j p_j g_j^\dagger \otimes \dots \otimes p_{n-1}$. Since only the j^{th} entry needs to be updated; reducing $g_j p_j g_j^\dagger$ can be done in constant time.

2.3 Limitation of extended stabilizer formalism

Applying non-Clifford gates increases the stabilizer rank of a stabilizer state $|\psi\rangle$, as generators evolve from single Pauli strings into linear combinations of Pauli strings.

When non-Clifford gates act on every qubit, a generator initially represented as a single Pauli string becomes a sum of n' Pauli strings, where n' can grow to 4^n . Subsequent gates require iterating over all n' Pauli strings, making the computation significantly slower than the state-vector approach which processes 2^n -complex amplitudes. Figure 1 illustrates the increasing complexity of generators due to non-Clifford and two-qubit gate applications.

Example 2 The generator $\mathbb{P}_1 = Z$ turn to be $\cos(\theta_1)X - \sin(\theta_1)\cos(\theta_2)Z + \sin(\theta_1)\sin(\theta_2)Y$ after $R_y(\theta_1)$ and $R_x(\theta_2)$ actions.

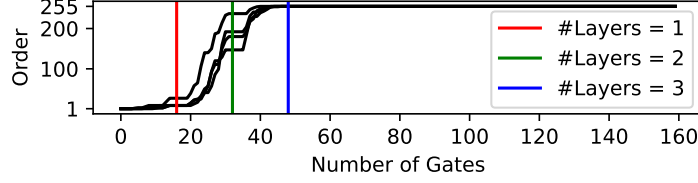


Fig. 1 The order n' on four generators is shown as four black lines, ranging from 1 to 4^4 . The gate application's order is from qubit 0^{th} to qubit $(n-1)^{\text{th}}$, left to right. We are considering the worst cases by using 4-qubit $|XYZ + \text{chain}\rangle$ ansatz, the circuit representation can be found in Fig. 2 (b).

3 Proposed techniques

3.1 Instruction

We present gates as instructions similar to Qiskit [2]. Each instruction is a tuple $\{g, w, \theta\}$, representing the gate name, qubit (wire), and parameter value (if applicable), respectively. For gate without parameters, θ is set as 0. Performing gate-by-gate on stabilizers leads to low performance; hence, we consider performing operators instead, where each operator contains gates of the same type. A quantum circuit is partitioned

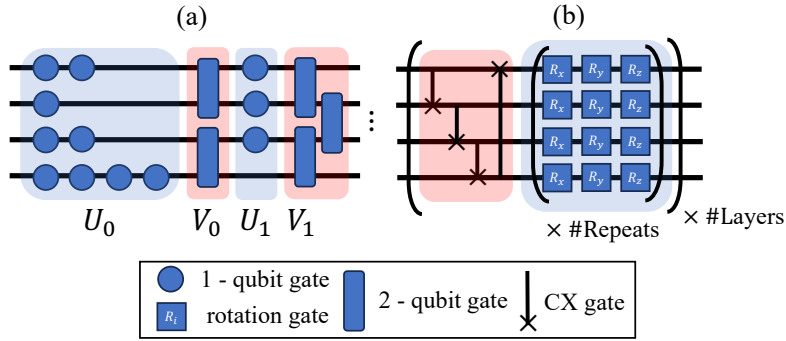


Fig. 2 (a) A quantum circuit can be divided into $\{U_k\}, \{V_k\}$, and end up with U_{K-1} or $V_{K'-1}$ $XYZ + W_{\text{chain}}$ topology.

into K U_k (only 1-qubit gates) and K' V_k (only 2-qubit gates) because the 2-qubit gate has different behavior from other gates. These operators interleaved each other, as presented in Fig. 2, obey $|K - K'| \leq 1$. The operator sequence is determined by the first instruction: if it is a single-qubit gate, the order will be $U_0, V_1, U_1, V_1, \dots$; otherwise, it starts with V_0 . Within each U_k , gates are further grouped by qubit, with $U_{k,j}$ denoting instructions in the k^{th} single-qubit operator acting on the j^{th} qubit. By grouping gates, there is no difference between Clifford and non-Clifford gates.

Rather than applying gates individually to the stabilizers, Qimax groups gates into operators and applies these operators collectively. The primary computational cost arises from updating Pauli strings, which involves transforming the j^{th} Pauli matrix in every Pauli string via conjugation. In the extended stabilizer formalism, applying m gates individually yields a time complexity of $\mathcal{O}(mn')$, where n' is the number of Pauli strings in the stabilizer representation. By grouping gates into K single-qubit operators and K' two-qubit operators, where $K + K' \ll m$, Qimax reduces the complexity to $\mathcal{O}((K + K')n')$. This reduction is effective because the number of operators is typically much smaller than $\#\text{Gates}$.

3.2 Encoding

We encode any Pauli string P_n as an integer index using base-4 with the mapping $I = 0, X = 1, Y = 2, Z = 3$. The index ranges from 0 (representing $I^{\otimes n}$) to $4^n - 1$ ($Z^{\otimes n}$). Conversely, decoding an index back to a Pauli string requires $\#\text{Qubits}$. When a non-Clifford gate acts on a Pauli matrix $p \neq I$ in P_n , it may transform into a linear combination $p = w_0X + w_1Y + w_2Z \equiv [w_0, w_1, w_2]$ as illustrated in Example. 1. We call w_j the weight of transformed generators. Since every Pauli matrix p_j in a generator may take this form, applying non-Clifford gates can transform a generator from a simple form $\mathbb{P}_n = \sum_j \lambda_j P_{n,j}$ (a sum of Pauli strings) to complex form $\hat{\mathbb{P}}_n = \sum_j \lambda_j \prod_{k=1}^n (\sum_l w_{k,l} p_{k,l})$, where the product is over qubits and the sum is over Pauli matrices, as shown in Example. 3.

The weight for \mathbb{P}_n are represented by a 3D tensor \mathbf{w} , where each entry $w \in \mathbf{w}$ satisfies $|w| \leq 1$ due to the normalization condition. In Qimax v2, \mathbf{w} is a fixed-size tensor padded with zeros, while in Qimax v3, it is a ragged tensor with corresponding indices \mathbf{i} to store only non-zero weights. In the worst case, where the number of Pauli strings $n' = 4^n$, the tensor \mathbf{w} has dimensions $4^n \times n \times 4$, corresponding to 4^n Pauli strings, n qubits and 4 Pauli matrices (I, X, Y, Z). Qimax v2 maintains a consistent tensor size for all cases, simplifying parallel computation, whereas Qimax v3 reduces unnecessary data but doubles memory usage due to the storage of indices \mathbf{i} . On the other hand, parallelizing computation on Qimax v2 is better than v3. The indices \mathbf{i} correspond to the coefficients $\boldsymbol{\lambda}$ in the simple form $\mathbb{P}_n = \sum_j \lambda_j P_{n,j}$ and have the same size as \mathbf{w} in the complex form.

We denote:

$$\begin{aligned} \Lambda &= [\boldsymbol{\lambda}_0, \dots, \boldsymbol{\lambda}_{n-1}], \boldsymbol{\lambda}_j \in \mathbb{R}^{n'} \\ \mathbf{W} &= [\mathbf{w}_0, \dots, \mathbf{w}_{n-1}], \end{aligned}$$

$$\mathbb{I} = [\mathbf{i}_0, \dots, \mathbf{i}_{n-1}].$$

are the scalars, weights, and corresponding indices for entire set of generators.

Example 3 $\hat{\mathbb{P}}_2 = 2(3Y + 4Z)Z + I(X + Z)$ is encoded as $\boldsymbol{\lambda} = [2, 1]$ and $\mathbf{w} = [[[0, 0, 3, 4], [0, 0, 0, 1]], [[1, 0, 0, 0], [0, 1, 0, 1]]]$ using one-hot encoding (Qimax v2). In the second approach, $\hat{\mathbb{P}}_2 \triangleq \begin{cases} \boldsymbol{\lambda} = [2, 1] \\ \mathbf{w} = [[[3, 4], [1]], [[1], [1, 1]]] \text{ (Qimax v3)} \\ \mathbf{i} = [[2, 3], [3]], [[0], [1, 3]] \end{cases}$. This complex form can be reduced to a simple form by multiple broadcasts between linear combinations. $\hat{\mathbb{P}}_2 \xrightarrow{\text{flatten()}}$
 $\mathbb{P}_2 = 6YZ + 8ZZ + IX + IZ \triangleq \begin{cases} \boldsymbol{\lambda} = [6, 8, 1, 1] \\ \mathbf{i} = [11, 15, 1, 2] \end{cases}$

3.3 Gate

3.3.1 1-qubit gate

Applying m single-qubit gates to the generator set G in a single step is more efficient than sequential application. This operation is notated as $\text{map}_{1q} : \mathbb{P} \times g^m \rightarrow \hat{\mathbb{P}}$ where \mathbb{P} is a generator and $\hat{\mathbb{P}}$ is its transformed form. Because map_{1q} only acts on X, Y or Z for every generator, we construct a look-up table called LUT_{1q} to track the output of every $\text{map}_{1q}(w, U_{k,j})$. LUT_{1q} is a tensor which has the shape $K \times n \times 3 \times 3$. As shown in Algorithm. 1, each $\text{map}_{1q}(\dots)$ is independent, enabling parallel computation. Constructing the LUT_{1q} can achieve a speedup of up to $K \times n \times 3$ times, depending on the number of available cores.

Algorithm 1 `create_LUT1q()`

Require: $\{U_{k,j}\}, K$
 $\text{LUT}_{1q} \leftarrow \mathbf{0}^{K \times n \times 3 \times 3}$
for k in $[0 \dots K - 1]$ **in [parallel] do**
 for j in $[0 \dots n - 1]$ **in [parallel] do**
 $i \leftarrow 0$
 for p in $[X, Y, Z]$ **in [parallel] do**
 $w \leftarrow \text{pauli_to_weight}(p)$
 for (g, wire, θ) in $U_{k,j}$ **do**
 $w \leftarrow \text{map}_{1q}(w, g(\theta))$
 end for
 $(\text{LUT}_{1q})_{k,j,i} \leftarrow w$
 $i \leftarrow i + 1$
 end for
 end for
end for
return LUT_{1q}

3.3.2 2-qubit gate

For simply, we consider the CX gate, which acts on a control qubit (indexed by c) and a target qubit (indexed by t), modifying the c^{th} and t^{th} Pauli matrices in each Pauli string $P_{n,j}$. The CX gate transforms these Pauli matrices according to specific rules, such as: $XI \leftrightarrow XX, IY \leftrightarrow ZY, YI \leftrightarrow YX, IZ \leftrightarrow ZZ, XY \leftrightarrow YZ$ while leaving II, IX, ZI and ZX unchanged, or change both Pauli and sign ($XZ \leftrightarrow -YY$). For m' CX gates, each Pauli string is updated according to these rules m' times. These transformations are efficiently implemented using a lookup table, as shown below:

$$\text{LUT}_c = \begin{bmatrix} 0 & 0 & 3 & 3 \\ 1 & 1 & 2 & 2 \\ 2 & 2 & 1 & 1 \\ 3 & 3 & 0 & 0 \end{bmatrix}, \text{LUT}_t = \begin{bmatrix} 0 & 1 & 2 & 3 \\ 1 & 0 & 3 & 2 \\ 1 & 0 & 3 & 2 \\ 0 & 1 & 2 & 3 \end{bmatrix}, \text{LUT}_{\text{sign}} = \begin{bmatrix} 1 & 1 & 1 & 1 \\ 1 & 1 & 1 & -1 \\ 1 & 1 & -1 & 1 \\ 1 & 1 & 1 & 1 \end{bmatrix}. \quad (5)$$

The transformed Pauli matrices and sign for the control (c^{th}) and target (t^{th}) qubits of a CX gate are obtained from $\text{LUT}_{c/t/\text{sign}}$. Unlike single-qubit gates, which may produce weighted sums of Pauli strings, two-qubit gates like CX require the generator to be in a simple form before application. This operation is denoted as $\text{map}_{2q} : \mathbb{P} \times \{g_1, \dots, g_m\} \rightarrow \mathbb{P}$, where \mathbb{P} is a generator and $\{g_1, \dots, g_m\}$ represents m two-qubit gates, preserving the simple form of the output.

4 Main algorithm

Algorithm 2 Qimax v3. For v2, the indices tensor \mathbb{I} is ignored.

Require: instructions, n
 $\{U_{k,j}\}, \{V_j\}, K, K' \leftarrow \text{divide_instruction}(\text{instructions})$
 $\text{order} \leftarrow \text{create_chain}(K, K'); \text{LUT}_{1q} \leftarrow \text{create_LUT}_{1q}(\{U_{j,i}\})$
 $\Lambda^{(0)}, \mathbb{I}^{(0)} \leftarrow [\text{create_Z}_j(j, n) \text{ for } j \text{ in } [0, n]]; j \leftarrow 0$
for order in orders **do**
 $k \leftarrow j \div 2$
 if order == 0 **then** $\triangleright \{U_{k,j}\}$
 $\Lambda, \mathbf{W}, \mathbb{I} \leftarrow \text{sub}(\Lambda^{(t)}, \mathbb{I}^{(t)}, \text{LUT}_{1q}[k])$
 $\Lambda^{(t+1)}, \mathbb{I}^{(t+1)} \leftarrow \text{flatten}(\Lambda, \mathbf{W}, \mathbb{I})$
 else $\triangleright \{V_k\}$
 for c, t in V_k **do** \triangleright Control and target wires
 $\Lambda^{(t+1)}, \mathbb{I}^{(t+1)} \leftarrow \text{map}_{2q}(\Lambda^{(k)}, \mathbb{I}^{(k)}, c, t)$
 end for
 end if
 $j \leftarrow j + 1$
end for
return $\{\Lambda^{(K+K')}, \mathbb{I}^{(K+K')}\}$

The initial generators $\{P_{n,j}^{(0)}\} = \{\mathbb{Z}_{n,j}\}$ are encoded in simple form:

$$\Lambda = \underbrace{[1, 1, \dots, 1]}_n, \quad \mathbb{I} = \underbrace{[[3], [3], \dots, [3]]}_n, \quad (6)$$

as defined in Eq. 1, where Λ represents the coefficients (all 1) and \mathbf{P} encodes the Pauli Z (index 3). In Qimax, the output of a single-qubit operator U_k serves as the input to the next two-qubit operator V_k , and vice versa, until the final operator is applied. The function `sub()` (for single-qubit gate substitution) and `map2q()` (for two-qubit gate permutations) have low computational complexity due to their reliance on lookup tables. However, the primary computational bottleneck arises from the `flatten()` function, which converts generators from complex forms to simple forms.

$$\text{flatten} : \hat{\mathbb{P}}_{n,j}^{(t)} \rightarrow \mathbb{P}_{n,j}^{(t)} = \sum_{k=0}^{n'-1} \left\{ \left(\bigotimes_{j=0}^{n-1} \mathbf{w}_{j,k}^{(t)} \right) \right\}, \quad (7)$$

where \otimes is Cartesian product notation. The function computes n' combinations of weights from the tensor $\mathbf{w}^{(t)}$, where $\mathbf{w}_{j,k}^{(t)}$ represents the weights for the j^{th} qubit in the k^{th} Pauli string. This involves iterating over all combinations of weights across qubits, with coefficients λ_k derived from the product of weights. Since single-qubit gates preserve the identity Pauli I , the number of combinations is reduced by a factor of $(3/4)^{n_I}$ for a Pauli string $P_{n,k}$ containing n_I Pauli I operators, as I contributes no additional terms.

5 Implementation

The three modes of Qimax are implemented in Python 3.10.11, using CuPy-cuda12x 13.4.0 [12] as the backend for GPU acceleration. Computationally intensive functions are executed in CUDA kernels with a block size of 256 and a grid size of $\lceil (\text{total elements} + 255) / 256 \rceil$, where total elements represent the number of tensor entries or tasks. The code and data for this study are accessible at <https://github.com/NAIST-Archlab/qimax-soft>.

Qimax v1 implements the extended stabilizer formalism without encoding or GPU parallelization, serving as a CPU-based baseline with limited scalability. Qimax v2 uses a fixed-size weight tensor of dimensions $n \times n' \times n \times 4$. This structure simplifies memory allocation but consumes significant memory during the `flatten()` function due to the exponential number of Pauli string combinations. Qimax v3, however, employs a ragged weight tensor with a corresponding index tensor \mathbf{i} , reducing memory usage by ignoring zero-padding. This enables v3 to handle sparse representations efficiently, though it requires additional memory for storing indices.

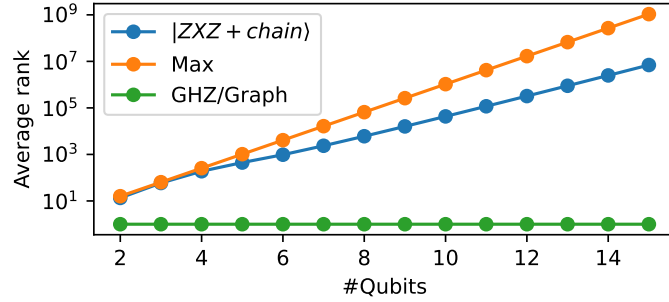


Fig. 3 The average stabilizer rank between circuit, while $|XYZ + chain\rangle$ and max stabilizer rank increase exponential ($\mathcal{O}(2^n)$ and $\mathcal{O}(4^n)$), GHZ and Graph are fixed as 1.

6 Experiments

Comparable software includes PennyLane 0.41.0 [13] and Qiskit 1.1.1 [2], both accelerated with NVIDIA’s cuQuantum SDK (lightning.gpu 0.41.0 and cusvader_simulator_statevector 0.13.3, respectively). Experiments were conducted on an Intel i9-10940X CPU (3.30 GHz) and an NVIDIA RTX 4090 GPU. Execution time was measured from the initialization of stabilizer generators to the computation of final generators. Each experiment was run at least 10 times, and the average execution time was calculated. The benchmarked circuits include the GHZ circuit (multi-qubit entangled state), Graph circuit (graph-based quantum state), and $|XYZ + chain\rangle$, as shown in Figure 2 (b). The circuit structure consists of L layers, with the XYZ component repeated $\#Repeats$ times within each layer. Experiments varied $\#Repeats$ from 100 to 100,000 to evaluate Qimax’s scalability. The $\#Gates$ increases linearly with $\#Repeats$ and $\#Qubits$. The average stabilizer rank of generators, which impacts performance, is plotted in Figure 3; higher ranks correspond to lower performance in Qimax due to increased computational complexity.

Qimax v1 shares properties with other stabilizer formalism packages, such as Stim [8], enabling the simulation of many-qubit Clifford circuits in seconds, as shown in Figure 4, in this cases, GHZ and Graph circuit has the average stabilizer rank as 1. However, Qimax v1 is slower than Stim due to its support for non-Clifford gates, prioritizing functionality over performance. Qimax v3 demonstrates superior performance in experiments with large $\#Repeats$, as shown in Figure 5, outperforming GPU-accelerated Qiskit and PennyLane. At higher $\#Repeats$, Qimax v3’s performance advantage over these packages increases significantly. CPU-based versions of all packages exhibit the longest execution times, with Qiskit generally outperforming PennyLane. All packages exhibit exponential scaling with $\#Qubits$ due to the state-vector size (for Qiskit and PennyLane) or the increase in gate count and average stabilizer rank (for Qimax).

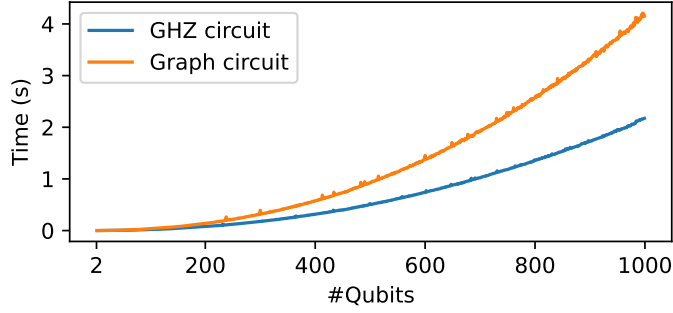


Fig. 4 The execution time for GHZ circuit and graph circuit on Qimax, these circuits are generated from MQT Bench [14].

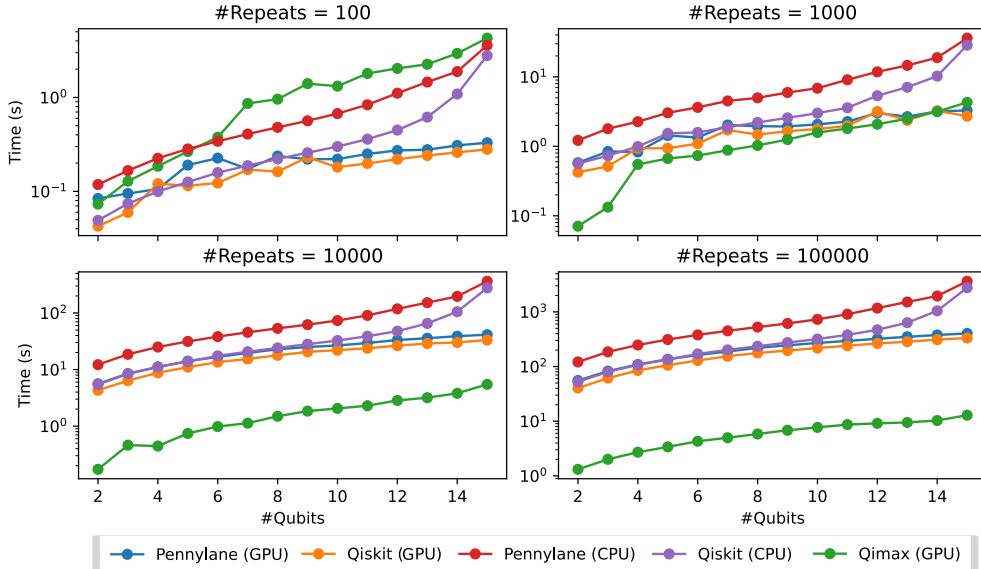


Fig. 5 Execution time from different versions of Pennylane, Qiskit, and Qimax. The y-axis is plotted on logarithmic scale. The range of #Qubits is 2 to 15.

7 Conclusion

The Qimax is the parallel version of stabilizer formalism using encoding-decoding architecture. While operating on multi-dimensional tensor speed-up by both software and hardware rather than the original stabilizers, Qimax can take advantage of the GPU. This approach offers a short execution time in case of a thousand gates, faster than GPU-based Qiskit and Pennylane, and even Qimax is implemented by Python. For high-stabilizer rank circuits, Qimax will be slower than the state-vector simulator due to the squared complexity ($\mathcal{O}(4^n)$ compared to $\mathcal{O}(2^n)$), same as others extended stabilizer formalism. The next versions focus on optimizing multiple circuits' execution.

In this work, we introduced Qimax, a high-performance quantum circuit simulator that advances the extended stabilizer formalism through a novel encoding-decoding architecture optimized for parallel computation. By representing stabilizer generators as multi-dimensional tensors and leveraging GPU acceleration via CuPy and CUDA, Qimax achieves significant speedups compared to traditional extended stabilizer formalism. This approach enables Qimax to efficiently handle both Clifford and non-Clifford gates. Experimental results demonstrate that Qimax, particularly its v3 mode with ragged tensor encoding, outperforms GPU-accelerated state-vector simulators with millions of gates, especially in scenarios with large numbers of repeated circuit layers.

However, Qimax’s performance is sensitive to the stabilizer rank of the simulated circuits. For high-rank circuits, where n' approaches the worst-case bound of 4^n , Qimax’s computational complexity scales as $\mathcal{O}(4^n)$, compared to $\mathcal{O}(2^n)$ for state-vector simulators. This limitation, common to other extended stabilizer formalism packages, arises from the exponential growth of Pauli string combinations during operations like the `flatten()` function. Despite this, Qimax v3 mitigates memory constraints through sparse tensor representations, enabling it to handle a broader range of circuits than its fixed-tensor counterpart (v2). Future versions of Qimax will focus on further optimizing the execution of multiple circuits in parallel, enhancing scalability for variational quantum algorithms and quantum machine learning workloads. Additional improvements will target the `flatten()` bottleneck by exploring advanced tensor contraction techniques and hybrid CPU-GPU workflows. By continuing to refine its architecture and algorithms, Qimax aims to bridge the gap between stabilizer-based and state-vector simulators, offering a robust and efficient platform for quantum circuit simulation in both research and practical applications.

Acknowledgements. This research was supported by the VNUHCM - University of Information Technology’s Scientific Research Support Fund.

Appendix A Utilities function used in three mode

The Qimax v2 and v3 use different encoders. v2 encode Pauli matrix and summation of Pauli matrix as the same 4D vector; in specially, it considers a single Pauli matrix as a 1-term sum. Both modes encode the Pauli string as an integer using base 4. We summarize all other functions as:

- `pauli_to_index(p)` and `index_to_pauli(i)`: Encode a Pauli $\{I, X, Y, Z\}$ as an integer $\{0, 1, 2, 3\}$ and vice versa.
- `pauli_to_weight(p)` and `weight_to_pauli(w)`: Encode a Pauli $\{I, X, Y, Z\}$ as an one-hot vector e_j and vice versa.
- `word_to_index(P)` and `index_to_word(P, n)`: Encode a Pauli word as integer using base-4. On the other hand, we need an additional parameter `#Qubits`.
- `index_to_indices(i)` and `indices_to_index(I)`: Convert an encoded Pauli word (integer form) to array form and vice versa. For example: $27(XYZ) \rightarrow [1, 2, 3]$.
- `create_Zj(j, n)`: Return n -dim one-hot vector e_j .
- `create_chain(K, K')`: Create the chain $[1, 0, 1, \dots]$ if the instructions begin with a 1-qubit gate and vice versa.

- divide_instruction (instruction): Split the instruction into $\{U_{j,i}\}$ and $\{V_j\}$, K and K' are two corresponding first dimensional.

Appendix B Data for constructing 1-qubit lookup table

The non-native gate used in above experiments are presented in Table. B1. Noted that this table can be expanded for any gates.

g	$\lambda P^{(t)}$	$\lambda P^{(t+1)}$	$w^{(t+1)}$
H	X	Z	$[w_2, -w_1, w_0]$
	Y	$-Y$	
	Z	X	
S	X	Y	$[w_1, w_0, w_2]$
	Y	X	
X	Z	$-Z$	$[w_0, w_1, -w_2]$
SX	Y	Z	$[w_0, -w_2, w_1]$
	Z	$-Y$	
$R_x(\theta)$	Y	$\cos(\frac{\theta}{2})Y + \sin(\frac{\theta}{2})Z$	$[w_0, w_1 \cos(\theta) - w_2 \sin(\theta), w_1 \sin(\theta) + w_2 \cos(\theta)]$
	Z	$\cos(\frac{\theta}{2})Z - \sin(\frac{\theta}{2})Y$	
$R_y(\theta)$	X	$\cos(\frac{\theta}{2})X - \sin(\frac{\theta}{2})Z$	$[w_0 \cos(\theta) + w_2 \sin(\theta), w_1, w_2 \cos(\theta) - w_0 \sin(\theta)]$
	Z	$\cos(\frac{\theta}{2})Z + \sin(\frac{\theta}{2})X$	
$R_z(\theta)$	X	$\cos(\frac{\theta}{2})X + \sin(\frac{\theta}{2})Y$	$[w_0 \cos(\theta) - w_1 \sin(\theta), w_1 \cos(\theta) + w_0 \sin(\theta), w_2]$
	Y	$\cos(\frac{\theta}{2})Y - \sin(\frac{\theta}{2})X$	

Table B1 Quantum gate operations and results with $w^{(t)} = [w_0, w_1, w_2]$ on $\{H, S, X, SX, R_x(\theta), R_y(\theta), R_z(\theta)\}$. The unchanged cases are ignored.

Appendix C Single-qubit Pauli measurement

Let $\mathbb{P}_{n,k,b} = \underbrace{I \otimes \cdots \otimes |b\rangle\langle b|_k \otimes \cdots \otimes I}_{n \text{ terms}} = \frac{1}{2}((-1)^b Z_{n,k} + I^{\otimes n})$ for $k \in [n]$. When mea-

suring the k^{th} qubit of an n -qubit state $|\psi\rangle$ using projectors $\{\mathbb{P}_{n,k,0}, \mathbb{P}_{n,k,1}\}$, we get two possible outcomes: 0 with probability $p_{k,0}$ and 1 with probability $p_{k,1}$. It follows that $p_{k,0} = \text{Tr}(\mathbb{P}_{n,k,0}|\psi\rangle\langle\psi|)$ where Tr is the trace mapping. As shown in (4), the density operator $|\psi\rangle\langle\psi|$ can be written using generators i.e., $|\psi\rangle\langle\psi| = \frac{1}{2^n} \sum_{\mathbb{P} \in G} \mathbb{P}$. The probability $p_{k,0}$ can be obtained as:

$$\begin{aligned} p_{k,0} &= \text{Tr}(\mathbb{P}_{n,k,0}|\psi\rangle\langle\psi|) \\ &= \text{Tr}\left(\frac{1}{2}(I^{\otimes n} + Z_{n,k})|\psi\rangle\langle\psi|\right) \end{aligned}$$

$$\begin{aligned}
&= \frac{1}{2} (\text{Tr}(|\psi\rangle\langle\psi|) + \text{Tr}(Z_{n,k}|\psi\rangle\langle\psi|)) \\
&= \frac{1}{2} + \frac{1}{2^{n+1}} \sum_{\lambda_{\mathcal{P}_n}} \lambda_{\mathcal{P}_n} \text{Tr}(Z_{n,k} \mathcal{P}_n)
\end{aligned}$$

For any Pauli string P_n , we can express $\text{Tr}(P_n)$ as $\text{Tr}(P_0) \cdots \text{Tr}(P_{n-1})$. Since $\text{Tr}(X) = \text{Tr}(Y) = \text{Tr}(Z) = 0$, $\text{Tr}(P_n) \neq 0$ if and only if $P_n = I^{\otimes n}$. Furthermore, $\mathbf{P} = Z_k$ if and only if $Z_k P_n = I^{\otimes n}$. Thus p_k can be simplified as $\frac{1}{2} + \frac{1}{2} \sum_{\mathcal{P}_n = Z_k} \lambda_{\mathcal{P}_n}$.

References

- [1] Arute, F., Arya, K., Babbush, R., Bacon, D., Bardin, J.C., Barends, R., Biswas, R., Boixo, S., Brandao, F.G.S.L., Buell, D.A., Burkett, B., Chen, Y., Chen, Z., Chiaro, B., Collins, R., Courtney, W., Dunsworth, A., Farhi, E., Foxen, B., Fowler, A., Gidney, C., Giustina, M., Graff, R., Guerin, K., Habegger, S., Harrigan, M.P., Hartmann, M.J., Ho, A., Hoffmann, M., Huang, T., Humble, T.S., Isakov, S.V., Jeffrey, E., Jiang, Z., Kafri, D., Kechedzhi, K., Kelly, J., Klimov, P.V., Knysh, S., Korotkov, A., Kostrița, F., Landhuis, D., Lindmark, M., Lucero, E., Lyakh, D., Mandrà, S., McClean, J.R., McEwen, M., Megrant, A., Mi, X., Michielsen, K., Mohseni, M., Mutus, J., Naaman, O., Neeley, M., Neill, C., Niu, M.Y., Ostby, E., Petukhov, A., Platt, J.C., Quintana, C., Riefel, E.G., Roushan, P., Rubin, N.C., Sank, D., Satzinger, K.J., Smelyanskiy, V., Sung, K.J., Trevithick, M.D., Vainsencher, A., Villalonga, B., White, T., Yao, Z.J., Yeh, P., Zalcman, A., Neven, H., Martinis, J.M.: Quantum supremacy using a programmable superconducting processor. *Nature* **574**(7779), 505–510 (2019) <https://doi.org/10.1038/s41586-019-1666-5>
- [2] Javadi-Abhari, A., al: Quantum computing with Qiskit (2024)
- [3] Bayraktar, al: cuquantum sdk: A high-performance library for accelerating quantum science. In: 2023 IEEE International Conference on Quantum Computing and Engineering (QCE), vol. 01, pp. 1050–1061 (2023). <https://doi.org/10.1109/QCE57702.2023.00119>
- [4] Vinkhuijzen, L., Coopmans, T., Elkouss, D., Dunjko, V., Laarman, A.: LIMDD: A Decision Diagram for Simulation of Quantum Computing Including Stabilizer States. *Quantum* **7**, 1108 (2023) <https://doi.org/10.22331/q-2023-09-11-1108>
- [5] Gidney, C.: Stim: a fast stabilizer circuit simulator. *Quantum* **5**, 497 (2021) <https://doi.org/10.22331/q-2021-07-06-497>
- [6] Mei, J., Bonsangue, M., Laarman, A.: Simulating quantum circuits by model counting. In: Gurfinkel, A., Ganesh, V. (eds.) *Computer Aided Verification*, pp. 555–578. Springer, Cham (2024)

- [7] Bravyi, S., Browne, D., Calpin, P., Campbell, E., Gosset, D., Howard, M.: Simulation of quantum circuits by low-rank stabilizer decompositions. *Quantum* **3**, 181 (2019) <https://doi.org/10.22331/q-2019-09-02-181>
- [8] Gidney, C.: Stim: a fast stabilizer circuit simulator. *Quantum* **5**, 497 (2021) <https://doi.org/10.22331/q-2021-07-06-497>
- [9] Kissinger, A., Wetering, J.: Simulating quantum circuits with zx-calculus reduced stabiliser decompositions. *Quantum Science and Technology* **7**(4), 044001 (2022)
- [10] Kissinger, A., Wetering, J.: PyZX: Large Scale Automated Diagrammatic Reasoning. In: Coecke, B., Leifer, M. (eds.) *Proceedings 16th International Conference on Quantum Physics and Logic*, Chapman University, Orange, CA, USA., 10–14 June 2019. *Electronic Proceedings in Theoretical Computer Science*, vol. 318, pp. 229–241. Open Publishing Association, ??? (2020). <https://doi.org/10.4204/EPTCS.318.14>
- [11] Osama, M., Thanos, D., Laarman, A.: Parallel equivalence checking of stabilizer quantum circuits on gpus. In: Gurfinkel, A., Heule, M. (eds.) *Tools and Algorithms for the Construction and Analysis of Systems*, pp. 109–128. Springer, Cham (2025)
- [12] Okuta, R., Unno, Y., Nishino, D., Hido, S., Loomis, C.: Cupy: A numpy-compatible library for nvidia gpu calculations. In: *Proceedings of Workshop on Machine Learning Systems (LearningSys) in The Thirty-first Annual Conference on Neural Information Processing Systems (NIPS)* (2017)
- [13] Bergholm, V., al: PennyLane: Automatic differentiation of hybrid quantum-classical computations (2022)
- [14] Quetschlich, N., Burgholzer, L., Wille, R.: MQT Bench: Benchmarking Software and Design Automation Tools for Quantum Computing. *Quantum* (2023) <https://doi.org/10.22331/q-2023-07-20-1062> [arxiv:2204.13719](https://arxiv.org/abs/2204.13719) [quant-ph]